RESEARCH ARTICLE | APRIL 09 2026

Single-shot quantitative differential phase contrast microscopy based on support-domain constraint

Tingxiang Xiong ; Yefeng Shu ; Ran Ye ; Maciej Trusiak ; Malgorzata Kujawinska ; Jiasong Sun ; Yao Fan ; Chao Zuo

APL Photonics 11, 046107 (2026)
https://doi.org/10.1063/5.0314921

Single-shot quantitative differential phase contrast microscopy based on support-domain constraint

Cite as: APL Photon. 11, 046107 (2026); doi: 10.1063/5.0314921
Submitted: 2 December 2025 • Accepted: 20 March 2026 •
Published Online: 9 April 2026

View Online Export Citation CrossMark

Tingxiang Xiong,[1,2,3] Yefeng Shu,[1,2,3] Ran Ye,[1,4] Maciej Trusiak,[5] Malgorzata Kujawinska,[5] Jiasong Sun,[1,2,3,a)] Yao Fan,[1,2,3,a)] and Chao Zuo[1,2,3,a)]

AFFILIATIONS

[1] Smart Computational Imaging Laboratory (SCILab), School of Electronic and Optical Engineering, Nanjing University of Science and Technology, Nanjing, Jiangsu Province 210094, China
[2] Smart Computational Imaging Research Institute (SCIRI) of Nanjing University of Science and Technology, Nanjing, Jiangsu Province 210019, China
[3] Jiangsu Key Laboratory of Visual Sensing & Intelligent Perception, Nanjing, Jiangsu Province 210094, China
[4] School of Computer and Electronic Information, Nanjing Normal University, Nanjing, Jiangsu Province 210023, China
[5] Warsaw University of Technology, Institute of Micromechanics and Photonics, 8 Sw. A. Boboli Street, Warsaw 02-525, Poland

[a)] **Authors to whom correspondence should be addressed:** sunjiasong@njust.edu.cn; fanyao@njust.edu.cn; and zuochao@njust.edu.cn

ABSTRACT

Differential phase contrast (DPC) microscopy is a powerful non-interferometric quantitative phase imaging (QPI) technique widely used for label-free visualization of transparent specimens under partially coherent illumination. However, its reliance on multi-frame acquisitions to ensure isotropic phase reconstruction inherently limits imaging speed, hindering the observation of fast biological dynamics. Here, we present support-domain-constraint DPC (SDC-DPC), a single-shot, isotropic-resolution QPI method that reconstructs quantitative phase maps from only one raw intensity image. By employing an optimized uniform semi-ring illumination to enhance the uniformity of the phase transfer function and incorporating a spatial support constraint into an iterative reconstruction framework, SDC-DPC compensates for the missing frequency components and suppresses the directional artifacts inherent to single-directional DPC. Simulations and experiments demonstrate that SDC-DPC achieves phase reconstruction accuracy and resolution comparable to conventional four-frame DPC for both static and dynamic samples, while completely eliminating motion artifacts in live-cell imaging. This work establishes a simple yet powerful paradigm that transforms DPC into a single-shot quantitative phase microscopy modality, opening new avenues for label-free imaging of dynamic biological processes.

I. INTRODUCTION

Quantitative Phase Imaging (QPI), as a label-free optical technique, enables high-content dynamic analysis of live cells while avoiding phototoxicity and photobleaching.[1] Unlike traditional phase contrast microscopy,[2] which only provides qualitative contrast, QPI combines the visualization of transparent samples with the capability for quantitative measurement of phase information. Therefore, it holds significant potential for application in monitoring cellular physiological processes, drug screening, and pathological analysis. Over the past few decades, the QPI technology system has continuously evolved, leading to the emergence of various typical implementation approaches, including Digital Holographic Microscopy (DHM),[3,4] four-wave lateral shearing interferometry,[5–7] Diffraction Phase Microscopy (DPM),[8] Transport of Intensity Equation (TIE),[9] Differential Phase Contrast (DPC),[10–15] Fourier Ptychographic Microscopy (FPM),[16,17] and imaging methods based on the Kramers–Kronig relations.[18,19] These

methods, each with unique features in theoretical models, optical configurations, and computational inversion strategies, have collectively driven the transition of QPI from qualitative observation to quantitative measurement.

Non-interferometric QPI techniques have gained increasing attention for their robustness and experimental simplicity. By introducing controlled asymmetry into the imaging system through defocus modulation[9] or asymmetric illumination, they establish a measurable mapping between sample phase and image intensity.[20,21] In particular, DPC stands out for its inherent compatibility with partially coherent illumination, offering speckle-free imaging, high stability, and resolution beyond twice the coherent diffraction limit. It modulates the sample's phase gradient information into detectable intensity variations. Under the weak object approximation, the relationship between intensity and phase is linearized and characterized by an asymmetric phase transfer function (PTF), enabling quantitative phase recovery through deconvolution.[22] However, under single-axis illumination, the PTF exhibits zero response along the asymmetric axis, resulting in missing frequency components that cannot be effectively transferred to the intensity domain. This incomplete spectral coverage fundamentally limits single-axis DPC from achieving fully reconstructive phase imaging and leads to directional information loss.[23]

To overcome this issue, conventional DPC typically employs multi-axis illumination strategies to compensate for spectrum deficiencies and achieve more comprehensive frequency coverage. Among these, two-axis orthogonal illumination is considered the minimum configuration required for complete phase reconstruction. Building on this foundation, several optimized illuminations have been proposed by analyzing the relationship between the illumination function and the PTF to achieve a more uniform spectrum response.[24–27] For example, the optimal illumination can produce smoother phase transfer responses within the theoretical bandwidth ($2NA_{obj}/\lambda$), thereby enabling nearly isotropic phase recovery performance. However, DPC still requires illumination along at least two axes to synthesize a frequency spectrum that comprehensively covers all spatial directions. This inherent dependence limits its temporal resolution and consequently restricts its applicability in high-speed, high-spatiotemporal-resolution dynamic imaging scenarios.

In recent years, with the continuous deepening of live-cell dynamics research, QPI technology is moving toward millisecond-level high-speed imaging, prompting researchers to explore the feasibility of single-shot QPI. Existing ideas primarily rely on multi-channel multiplexing strategies, where the multi-frame information under multi-axis illumination is encoded into different signal channels during a single exposure, and then, the multi-axis information is recovered through signal separation. Typical schemes include utilizing tristimulus light source channels (such as color LED arrays[23,28–30] or color filters[31]) to achieve different illumination patterns and using a Bayer-filtered color camera to capture the synthesized intensity image. However, this method is susceptible to color crosstalk, and the sample's dispersion characteristics can further reduce the accuracy of phase measurement. Another scheme involves combining a polarization camera with a four-directional polarization film to achieve single-exposure DPC, but its system structure is complex and significantly reduces the imaging field of view.[32,33] Furthermore, schemes based on wavelength- or polarization-based multiplexing reduce the effective spatial resolution of the detector and may introduce pixel aliasing issues. More critically, these approaches fundamentally rely on the information multiplexing of multi-axis illumination, leading to substantial redundancy in data sampling. To date, the theoretical limits of DPC phase reconstruction have not been investigated from the perspective of information theory and minimal data redundancy.

This paper proposes a single-shot isotropic resolution DPC based on support-domain constraint [Support Domain Constraint DPC (SDC-DPC)], which achieves single-exposure QPI without relying on any illumination multiplexing, while minimizing data redundancy. We design an optimal semi-ring illumination to minimize the near-zero response region in the PTF, thereby obtaining more uniform spectrum coverage under single illumination. Furthermore, a spatial support-domain constraint is introduced as a physical prior, effectively compensating for the missing frequency caused by the residual zero response. Through iterative optimization and refinement of the initial support domain, SDC-DPC achieves a balance between artifact suppression and detail fidelity, thus accurately recovering the sample's quantitative phase distribution. Experimental results demonstrate that SDC-DPC can obtain high-quality phase reconstruction results comparable to traditional dual-axis DPC in both fixed samples and dynamic live-cell imaging, while achieving a fourfold increase in frame rate. This study systematically reveals the feasibility of single-frame non-interferometric QPI from the perspective of minimizing information redundancy, opening up a new direction for high-speed, label-free cell imaging.

II. ANALYSIS OF PTF UNIFORMITY UNDER DIFFERENT ASYMMETRIC ILLUMINATION PATTERNS

Non-interferometric QPI techniques introduce an approximate object model to linearize the relationship between intensity and phase. The PTF quantitatively characterizes this relationship, and its response determines the performance of phase reconstruction. To achieve raw images with pronounced phase contrast and nearly isotropic resolution under a single illumination pattern, we first conducted a systematic analysis of the PTF characteristics under asymmetric illuminations. Based on the partially coherent imaging model under the weak object approximation, the PTF can be expressed as

$$PTF(\mathbf{u}) = \iint S(\mathbf{u_j})\left[P^*(\mathbf{u_j})P(\mathbf{u_j}+\mathbf{u}) - P(\mathbf{u_j})P^*(\mathbf{u_j}-\mathbf{u})\right]d^2\mathbf{u_j}, \quad (1)$$

where $\mathbf{u} = (u_x, u_y)$ is the spatial frequency coordinate, $\mathbf{u_j}$ denotes the source-plane spatial frequency, $P(\mathbf{u})$ is the objective pupil function, and $S(\mathbf{u})$ represents the intensity distribution of the source pattern shown in Fig. 1(a). In previous studies, the characteristics of the PTF under oblique illumination have been analyzed, and it has been demonstrated that employing optimized matched annular illumination in FPM and DPC can significantly enhance the transfer response across the entire $2NA_{obj}/\lambda$ bandwidth.[24–26] Based on the uniformity of the transfer function, metrics such as the signal-to-noise ratio and the isotropy of the synthetic PTF have been used to optimize the illumination patterns in two-axis DPC microscopy,

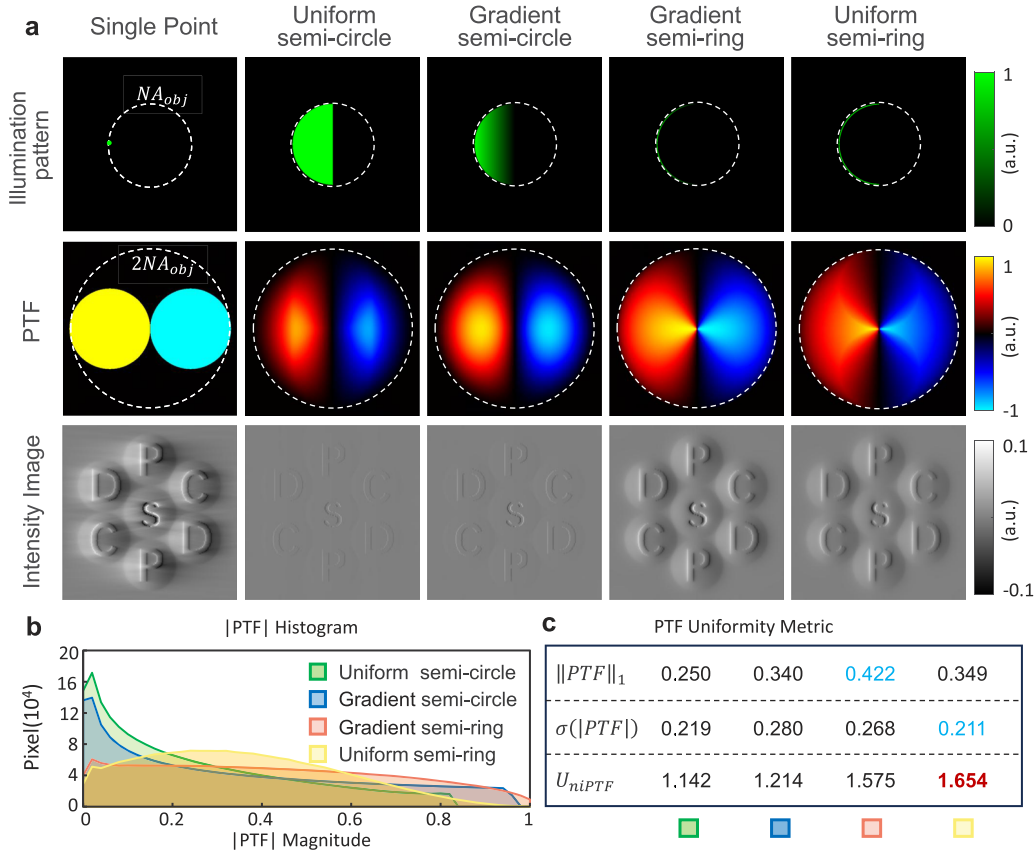

FIG. 1. Simulated PTFs under five illumination patterns and the evaluation of PTF uniformity. (a) Illumination patterns, simulated PTFs, and forward-propagated simulated intensity maps of a microlens array under the five illumination patterns: single-point, uniform semi-circle (radius R), gradient semi-circle (radius R), gradient semi-ring (width 0.01 R), and uniform semi-ring (width 0.01 R). (b) Histogram distributions of $|PTF|$ magnitudes for the latter four patterns. (c) PTF uniformity metric.

with strategies including gradient semi-ring illumination and gradient semi-circle illumination. However, a single illumination pattern cannot achieve a truly isotropic PTF, as its amplitude inevitably vanishes along certain asymmetric axes.

To address this challenge, we optimized the source pattern for a single asymmetric illumination to achieve a PTF with a more uniform distribution and minimal frequency loss. The DPC PTFs under five representative asymmetric illumination patterns, including single-point illumination, uniform semi-circle illumination,[10] gradient semi-circle illumination,[25] gradient semi-ring illumination,[24] and uniform semi-ring illumination (Fig. 1), are analyzed and compared to determine the optimal illumination pattern under single-axis conditions. The illumination pattern of SDC-DPC can be selected in any direction, and left-half illumination is taken as an example here. Under coherent single-point illumination, the PTF amplitude is constant (with a magnitude of 1), and its support domain consists of two tangent circle functions. While it generates strong phase contrast, it suffers from severe anisotropy. Reducing the illumination coherence (e.g., using uniform or gradient semi-circle sources) can extend the frequency domain coverage of the PTF but significantly weakens the low-frequency transfer and overall phase contrast. In contrast, both gradient and uniform semi-ring illuminations offer a superior compromise, improving PTF uniformity while balancing low-frequency response and high-frequency coverage [Fig. 1(a)]. Analysis of the PTF amplitude histograms indicates that uniform semi-ring illumination possesses the fewest pixels with near-zero amplitude, a characteristic crucial for robust phase retrieval [Fig. 1(b)]. The reduction in near-zero response areas implies less reliance on regularization during the deconvolution process, thereby allowing more frequency components to be accurately transferred to the intensity image without amplifying noise.

To quantitatively evaluate PTF uniformity across illumination patterns, we define the uniformity metric,

$$U_{niPTF} = \frac{\|PTF(\mathbf{u})\|_1}{\sigma(|PTF(\mathbf{u})|)}, \tag{2}$$

where $\|PTF(\mathbf{u})\|_1$ and $\sigma(|PTF(\mathbf{u})|)$ represent the mean and standard deviation of $|PTF(\mathbf{u})|$, respectively. This metric captures both the overall strength and the spatial uniformity of the PTF. Consistent with phase-contrast performance and histogram comparisons, semi-ring illumination clearly outperforms semi-circle illumination. In particular, uniform semi-ring illumination

($U_{niPTF} = 1.654$) surpasses gradient semi-ring illumination ($U_{niPTF} = 1.575$).

III. RECONSTRUCTION ALGORITHM OF SDC-DPC

Phase retrieval from intensity images acquired under DPC single-axis illumination can be formulated as an inverse problem. Such incomplete measurement scenarios can be addressed by introducing physical prior constraints to enhance the identifiability and stability of solutions. Prior constraints restrict the physical plausibility of the solution space, enabling convergence to an optimal solution consistent with the true sample even under underdetermined conditions.[34,35] Building upon this theoretical framework, we introduce support-domain constraint[36] during the iterative phase reconstruction process to address the issue of zero frequency response in specific directions of the PTF under single-axis DPC illumination. This constraint effectively reduces the uncertainty in the solution space by restricting the non-zero regions of the sample phase in the spatial domain and guides reasonable compensation of spectral information in missing directions during iterative inversion. In other words, the support domain provides a physical boundary condition consistent with the structural prior of the sample, enabling the algorithm to leverage spatial continuity and spectral consistency within known regions to extend limited measurement information into a self-consistent phase distribution across the full frequency range.

The SDC-DPC algorithm proposed in this paper aims to address the problem of dynamic phase imaging for colorless, transparent live cells. Given that the absorption of such cells is generally negligible, the algorithm is specifically optimized for pure-phase samples. Consequently, it does not require handling amplitude–phase coupling, but for the same reason, it is not suitable for samples with significant absorption. In the SDC-DPC algorithm, we employ an inverted optical path as shown in Fig. 2(a), select uniform semi-ring illumination as the illumination scheme, and acquire the corresponding single intensity map as an input for the algorithm. Figure 2(b) illustrates the reconstruction process using live-cell sample data as an example. First, an initial phase is estimated through single-step deconvolution applied to the intensity image,

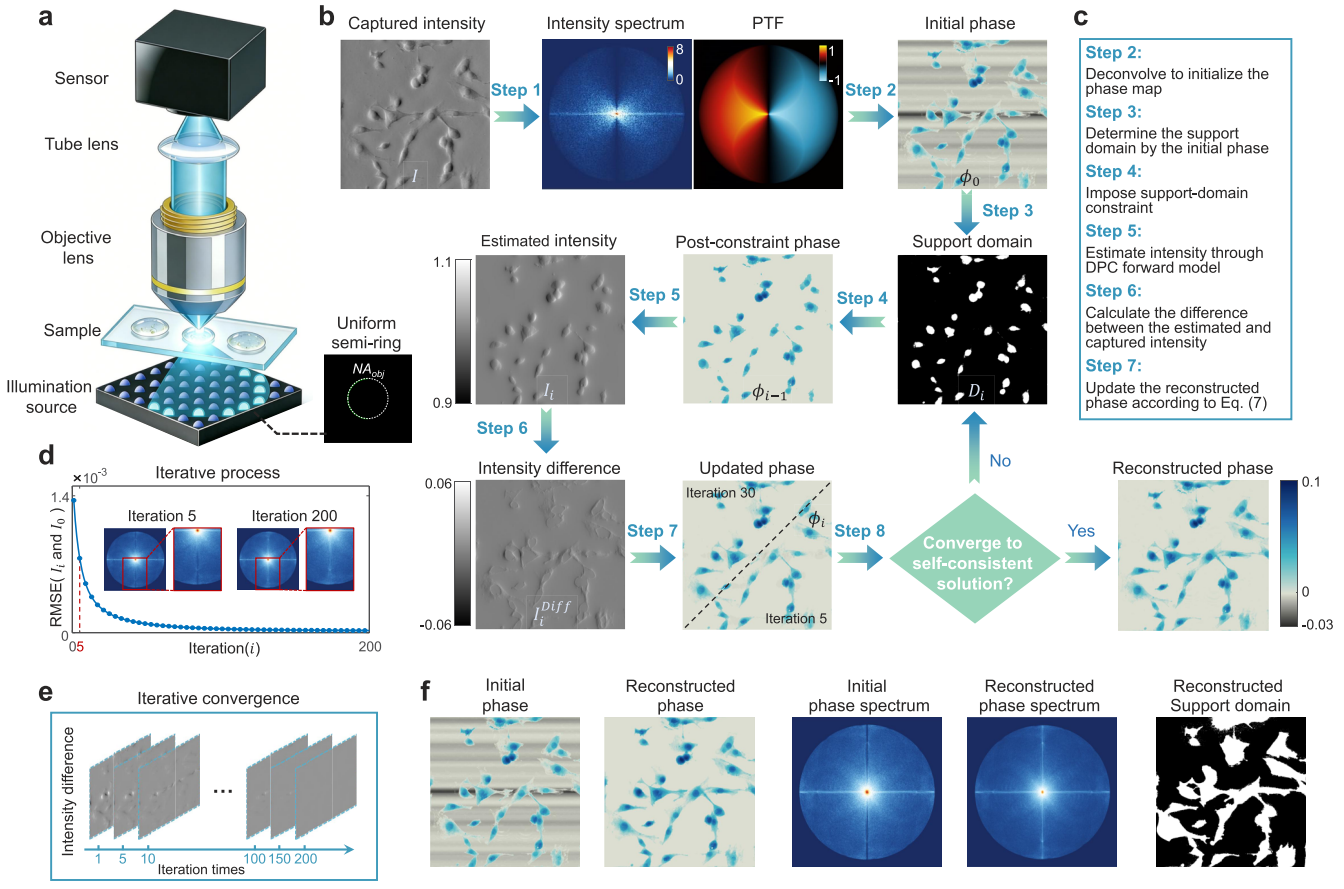

FIG. 2. Experimental setup and iterative phase retrieval workflow of the SDC-DPC algorithm. (a) Experimental setup with uniform semi-ring illumination. (b) Workflow of the SDC-DPC algorithm. (c) Introduction to several steps in (b). (d) RMSE convergence curve of estimated and captured intensities. (e) Intensity error convergence during iterations. (f) Iterative comparison between the initial input and the reconstructed output.

$$\phi_0(\mathbf{r}) = \mathscr{F}^{-1}\left\{\frac{PTF^*(\mathbf{u})\cdot\tilde{I}(\mathbf{u})}{|PTF(\mathbf{u})|^2+\beta}\right\}, \tag{3}$$

where $\mathbf{r} = (r_x, r_y)$ is the spatial coordinate and $\mathscr{F}^{-1}$ represents the 2D inverse Fourier transform. A Tikhonov regularization parameter β is introduced in the denominator of the deconvolution process to suppress noise amplification in low-response regions and enhance the stability of the solution. At this stage, since the PTF response approaches zero along a specific axis, the initial phase map exhibits pronounced directional artifacts [Fig. 2(b), step 2]. This result provides most of the phase edge information, which can be utilized to generate a binary support domain $D_i(\mathbf{r})$ through Otsu's adaptive thresholding segmentation or by constructing feature vectors based on gradient and intensity characteristics[37–41] [Fig. 2(b), step 3]. Thus, the support detection method achieves high-precision segmentation while maintaining low computational complexity. Subsequently, the support domain is applied to the phase map [Fig. 2(b), step 4] to force the background regions to zero,

$$\phi_{i-1}(\mathbf{r}) = \phi_{i-1}(\mathbf{r})\cdot D_i(\mathbf{r}). \tag{4}$$

Using the post-constraint phase, the DPC intensity image [Fig. 2(b), step 5] is then generated through the forward process,[42,43]

$$I_i(\mathbf{r}) = \mathscr{F}^{-1}\left\{\delta(\mathbf{u}) + PTF(\mathbf{u})\cdot\tilde{\Phi}_{i-1}(\mathbf{u})\right\}, \tag{5}$$

where $\delta(\mathbf{u})$ denotes the DC term, $\tilde{\Phi}_{i-1}(\mathbf{u})$ is the frequency-domain form of $\phi_{i-1}(\mathbf{r})$ after Fourier transform, and $I_i(\mathbf{r})$ denotes the estimated intensity image, which is used to calculate the residual intensity with respect to the actual acquired intensity [Fig. 2(b), step 6],

$$I_i^{Diff}(\mathbf{r}) = I_0(\mathbf{r}) - I_i(\mathbf{r}), \tag{6}$$

where $I_i^{Diff}(\mathbf{r})$ is the residual intensity. It is used to update the phase estimate so that it conforms to the captured intensity constraint [Fig. 2(b), step 7], according to

$$\phi_i(\mathbf{r}) = \phi_{i-1}(\mathbf{r}) + \alpha\cdot\mathscr{F}^{-1}\left\{\frac{PTF^*(\mathbf{u})\cdot\tilde{I}_i^{Diff}(\mathbf{u})}{|PTF(\mathbf{u})|^2}\right\}, \tag{7}$$

where α denotes the step size. The algorithm terminates upon residual convergence or after reaching the maximum iteration count, outputting the final cell phase map with high isotropy and fidelity, together with its spectral distribution [Figs. 2(d) and 2(e)]. The initial phase spectrum of one-step deconvolution shows diminished spectral magnitude along PTF-zero directions, producing prominent horizontal striping artifacts in the spatial domain. As iterations progress, spectral compensation gradually fills the zero-response regions along the symmetry axis and enhances signal intensity in weak-response regions, leading to progressive recovery of the missing horizontal structures, ultimately yielding a high-quality phase reconstruction with enhanced isotropy and effective noise suppression. Concurrently, the support domain converges toward its optimal domain through iterative updates of the phase map [Fig. 2(f)].

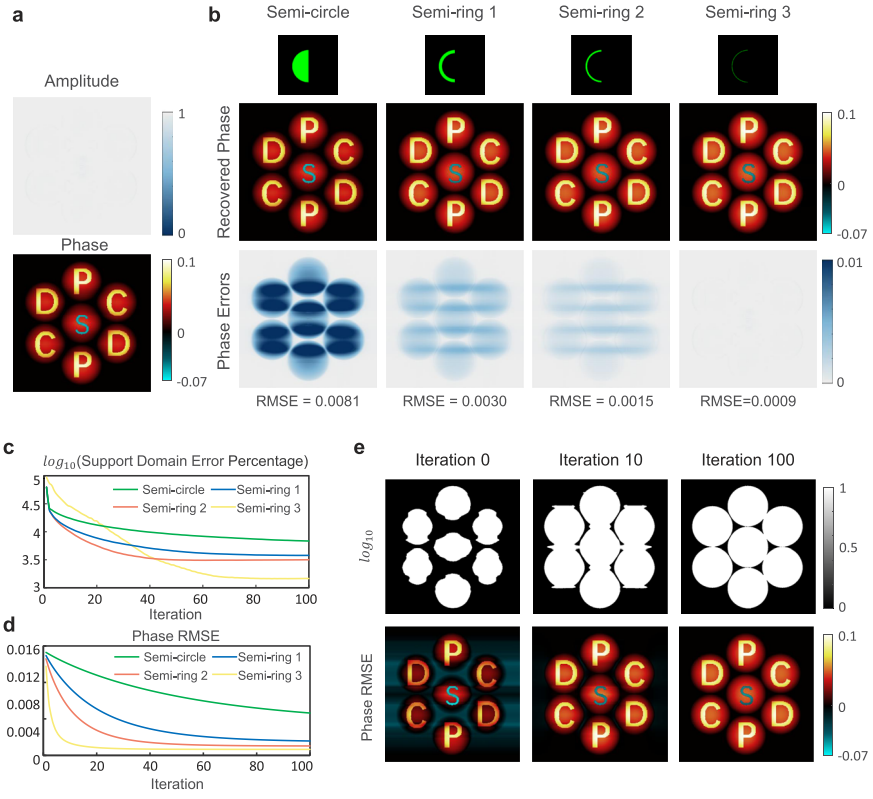

FIG. 3. SDC-DPC simulation results under uniform semi-circle and semi-ring illuminations with varying widths. (a) Amplitude and phase components of the simulated pure phase object. (b) Phase reconstruction results, phase reconstruction errors vs the ideal phase map and corresponding RMSE values after 100 iterations under the four illumination patterns: semi-circle, semi-ring (0.2 NA width), semi-ring (0.1 NA width), semi-ring (0.01 NA width). (c) $\log_{10}$ of the support-domain error rate over 100 iterations under the four illumination patterns. (d) Convergence curves of phase RMSE over 100 iterations under the four illumination patterns. (e) Support domains and the recovered phase maps at iteration 0, iteration 10, and iteration 100.

IV. SIMULATION VALIDATION OF SDC-DPC

To further validate the proposed SDC-DPC framework and analyze the effect of illumination coherence on reconstructed results, the reconstructions are performed in simulations under different illumination conditions [Fig. 3]. The phase component of the simulated pure sample has a phase range of 0–0.1 rad and consists of seven microlenses coated with different letters (positive phase: "D", "P", "C"; negative phase: "S") [Fig. 3(a)]. The simulated image is captured at 600 × 600 pixels with a pixel size of 0.294 μm, using an imaging wavelength of 510 nm and a 10×, 0.4 NA objective.

As shown in Fig. 3(b), in addition to the semi-circle illumination, the semi-ring widths are set to 0.2, 0.1, and 0.01 times the objective's NA. The phase error in the reconstruction decreases as the illumination coherence increases and is completely eliminated under the fourth quasi-coherent illumination. As discussed in Fig. 1, the simulation results demonstrate that a more uniform PTF facilitates improved phase reconstruction, guiding the selection of the optimal illumination pattern for experiments. In addition, the convergence curves for the support domain, shown in Fig. 3(c), reveal that the support domain cannot be accurately estimated under the first three illumination patterns, preventing effective phase reconstruction. Although the reconstructed phase map under the fourth illumination pattern achieves efficient convergence [Fig. 3(d)], it still requires at least 50 iterations to accurately estimate the support region and fully eliminate artifacts due to the anisotropic PTF distribution, as shown in the reconstructed support regions and phase maps after 10 and 100 iterations [Fig. 3(e)]. Overall, the simulation results validate that the phase information loss under a single DPC illumination pattern can be effectively compensated within the SDC-DPC framework under a semi-ring illumination pattern with a relatively narrow width. To demonstrate the noise robustness of the SDC-DPC algorithm under low signal-to-noise ratio conditions, relevant analyses and simulations are provided in Sec. S1 of the supplementary material.

In addition, the simulation experiments are conducted on a computer equipped with an Intel Core i5-12500H processor and 16 GB of RAM, without GPU acceleration. For the microlens array images used in this study, the reconstruction process involves 100 iterations. The results indicate that the reconstruction error stabilizes after ~50 iterations, with subsequent iterations primarily aimed at refining high-frequency details in the image. A complete reconstruction requires ~2–3 s. In practical applications, appropriate initialization can significantly reduce the number of iterations required. For example, in live-cell continuous imaging, the phase maps of cells between adjacent frames show minimal variation. By using the reconstruction result from the previous frame as the initial value for the next frame, except for the first frame, which underwent 100 iterations, all subsequent frames required only five iterations, decreasing the processing time to ~0.2–0.3 s. Future integration of GPU acceleration is expected to increase the reconstruction speed to 20 f/s, potentially enabling real-time live-cell dynamic imaging and reconstruction. Example reconstruction code for SDC-DPC is provided in Sec. S2 of the supplementary material.

V. EXPERIMENTAL RESULTS OF SDC-DPC ON FIXED AND DYNAMIC LIVE-CELL SAMPLES

The experimental setup is based on an inverted microscope (IX73, Olympus, Japan), with illumination arranged as a ring of 15 LEDs with a specified radius. The system employs a 10×, 0.4 NA objective lens and a 510 nm illumination wavelength. Image acquisition is performed using an industrial camera (The Imaging Source DMK 24UJ003) with a pixel size of 1.67 μm. The programmable LED array produces a semi-ring illumination pattern composed of

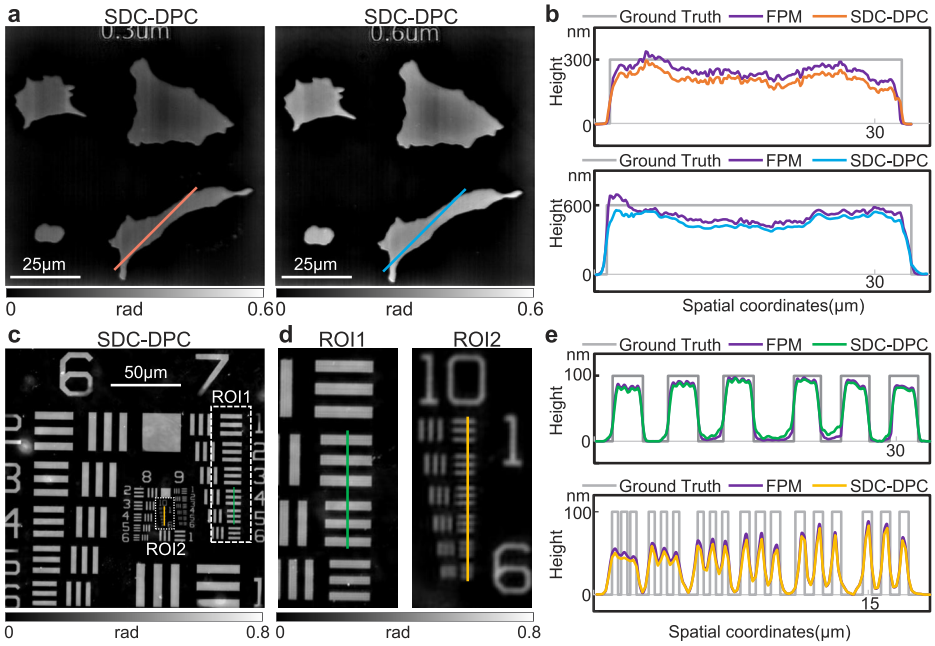

FIG. 4. Experimental results of the cell phantom and the pure-phase USAF resolution target. (a) Phase results of the cell phantom. (b) Phase values along the orange and blue lines indicated in (a). (c) Phase results of the pure-phase USAF resolution target. (d) Zoomed-in views of the sub-regions corresponding to the green (ROI 1) and yellow (ROI 2) lines in (c). (e) Phase values along the green and yellow lines in (d).

discrete LED elements, where the ring width corresponds to a single LED, with illumination coherence closely matching the fourth illumination condition in Fig. 4(a).

To demonstrate the effectiveness of SDC-DPC in quantitatively rendering a phase map without artifacts, we first apply the method to a fixed sample containing cell phantoms (Warsaw University of Technology) of heights 0.3 and 0.6 μm, as shown in Fig. 4(a), respectively. The refractive index of the sample material is 1.5668, with a refractive index-matching liquid of 1.51 applied between the glass slides. We additionally capture 12 frames of images for FPM reconstruction using 12 single-point LEDs arranged on a circle with the same radius as that used for uniform semi-ring illumination. The FPM results are used as a standard quantitative phase imaging reference for comparison. From the phase images, the overall imaging quality of FPM appears comparable to that of SDC-DPC, with no significant visual difference. Phase profiles for the two regions are shown in Fig. 4(b). The close agreement between the profiles demonstrates that SDC-DPC achieves phase reconstruction quality comparable to that of 12-frame FPM. To further validate the isotropic phase resolution of SDC-DPC, we apply the method to a phase USAF resolution target (Ready Optics—Latigo Optics Inc.) with a height of 100 nm, as shown in Fig. 4(c). The result shows no directional artifacts or resolution loss compared to the multi-frame DPC benchmark. The enlarged view in Fig. 4(d) and the corresponding profiles indicate that SDC-DPC achieves the theoretical maximum resolution of 328 nm, resolving up to group 10, element 4 of the target. Experimental results demonstrate that SDC-DPC achieves theoretical diffraction-limited resolution and delivers imaging quality comparable to that of multi-frame quantitative phase imaging techniques.

By reducing the image acquisition time of conventional DPC to one-fourth, SDC-DPC offers significant technical advantages for long-term quantitative observation of unstained live cells and

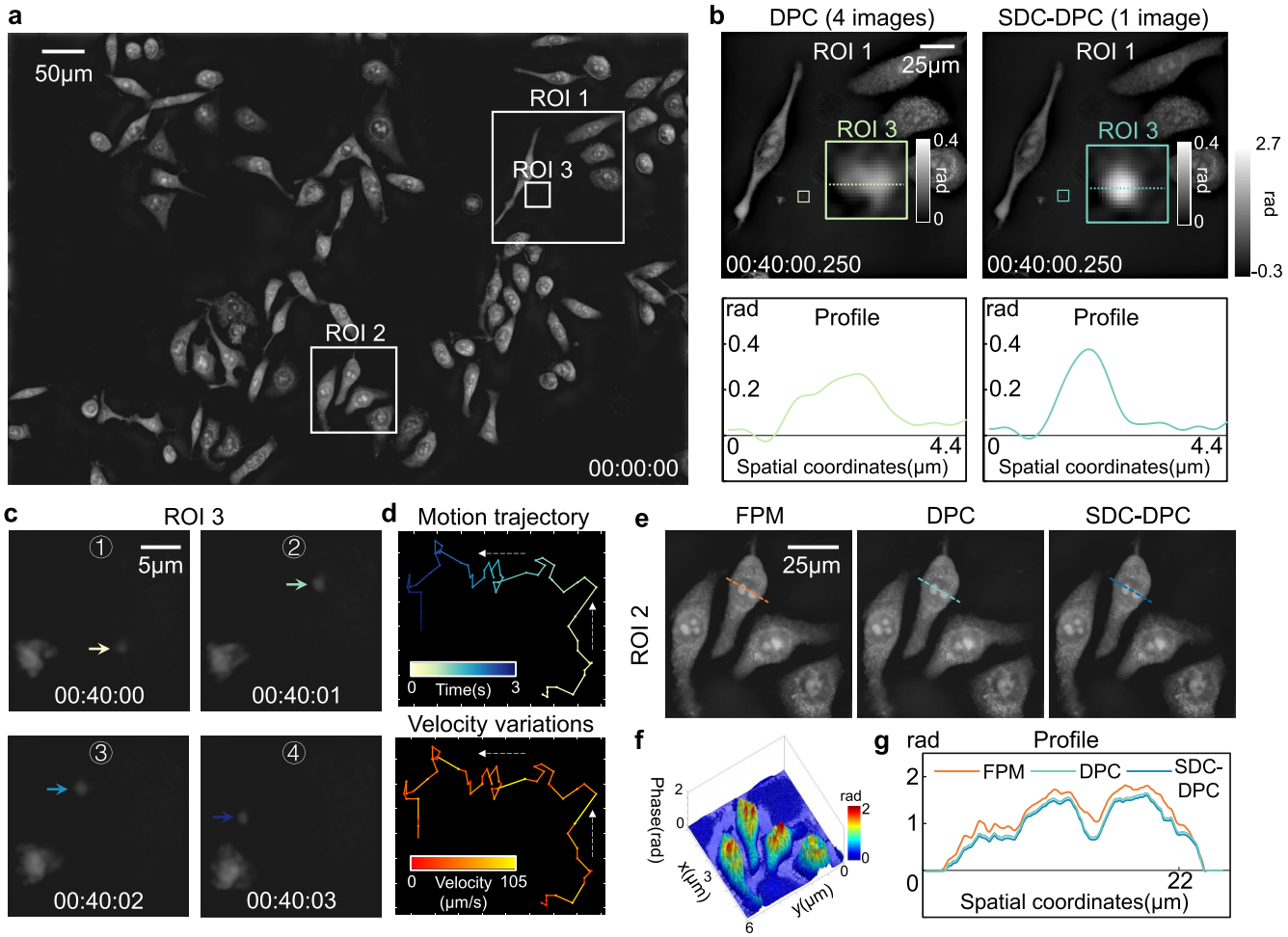

FIG. 5. SDC-DPC phase reconstruction results of HeLa cells over a 2-h period. (a) Full-field recovered phase result. (b) Phase reconstruction results of DPC and SDC-DPC in the same field of view, with line profile analysis performed on the suspended particles. (c) Dynamic tracking results of ROI 3 over 3 s. (d) Motion trajectory of suspended particles, and velocity variations at different positions. (e) Reconstruction results of FPM, DPC, and SDC-DPC in ROI 2. (f) 3D rendering results of ROI 2. (g) Phase value comparisons along line profiles in (e) (Multimedia available online). .

fast-moving objects. To demonstrate the effectiveness and superiority of the SDC-DPC method for live-cell imaging, we perform phase reconstruction on unstained HeLa cells over a 2-h period, as shown in Fig. 5 (Multimedia available online). In this experiment, HeLa cells were cultured in a 37 °C incubator with 5%CO_2 during revival and passaging and finally seeded in a 35 mm confocal dish for observation, with images acquired at a rate of 20 f/s. Figure 5(a) shows the first frame of the full-field reconstruction result. A sub-region (ROI 1) containing a rapidly moving suspended particle between 0 and 3 s during the 40th min is selected. Phase retrieval results for this region using both four-frame DPC and SDC-DPC at the same time point are compared in Fig. 5(b). The results show that while the HeLa cells exhibit slow movement with negligible morphological changes over this short interval, the fast-moving particle appears as a well-defined circle in the SDC-DPC reconstruction but becomes elongated in the four-frame DPC result. Furthermore, the phase profiles along its direction of motion reveal peak reduction, broadening, and significant motion artifacts in the four-frame DPC reconstruction compared to SDC-DPC. Further analysis of the fast-moving particle in ROI 1 over a 3-s period (60 frames) is shown in Fig. 5(c). Using SDC-DPC, we clearly observe its morphological changes along its motion trajectory over time and velocity variations at different positions [Fig. 5(d)]. This demonstrates that for rapidly moving targets, SDC-DPC, which requires only a single differential phase contrast image, effectively captures instantaneous morphology and accurate trajectories while avoiding motion artifacts.

In addition, before the 2-h experiment, we acquired 12 single-point FPM images, which allowed us to compare the initial cell state distribution among FPM, DPC, and SDC-DPC. Phase reconstructions of sub-region 2 (ROI 2) using FPM, four-frame DPC, and SDC-DPC are quantitatively compared [Fig. 5(e)], with Fig. 5(f) showing the corresponding 3D morphology. Analysis of the cellular phase profile [Fig. 5(g)] reveals that SDC-DPC achieves reconstruction accuracy comparable to that of four-frame DPC, although slightly inferior to FPM. These experimental results collectively demonstrate that SDC-DPC, utilizing only a single differential phase contrast image, enables high-resolution, long-term quantitative phase imaging of live cells.

VI. SUMMARY AND CONCLUSIONS

In summary, we have introduced a support-domain-constraint-based differential phase contrast microscopy technique to achieve single-shot, isotropic, quantitative phase imaging. Through the systematic evaluation of the PTFs across various asymmetric illumination geometries, we identify uniform semi-ring illumination as the optimal strategy due to its quasi-isotropic frequency response. Resolution target experiments quantitatively confirm that our method achieves diffraction-limited resolution without artifacts. Furthermore, long-term quantitative phase monitoring of live HeLa cells underscores the superior capability of SDC-DPC for real-time observation, enabling the clear visualization of rapidly moving cellular components without motion-induced blur.

Unfortunately, the effectiveness of this method strongly depends on the accurate determination of the sample's support domain, which becomes challenging when cells are overly confluent and lack a clear background. Simulation studies have confirmed that the current SDC-DPC method can achieve efficient phase retrieval for samples with a confluency of 50%. However, under extreme conditions, such as a confluency exceeding 90%, the lack of clear background regions makes it challenging to accurately determine the support domain, thereby limiting the method's ability to recover missing phase information.

Moreover, this study has validated the effectiveness of the support-domain constraint in compensating for missing phase information. Future work may proceed in two main directions. First, exploring the integration of the support domain as a regularization constraint into the reconstruction model could theoretically ensure convergence and yield more stable and efficient performance results in numerical simulations. Second, research could focus on embedding the SDC-DPC algorithm as a core module within a physics-driven deep learning network. This approach would not only leverage deep learning to enhance the robustness of SDC-DPC reconstruction and expand its applicability to dense samples, but also integrate additional spatial prior constraints within a unified physics-driven deep learning framework.

SUPPLEMENTARY MATERIAL

The supplementary material encompasses the following sections: S1: Supplementary simulations on the robustness of SDC-DPC; S2: Supplementary code for SDC-DPC.

ACKNOWLEDGMENTS

This work was supported by the National Key Research and Development Program of China (Grant Nos. 2024YFE0101300, 2022YFA1205002, 2024YFF0505603, and 2024YFF0505600), National Natural Science Foundation of China (Grant Nos. 62227818, 62361136588, 62305162, U21B2033, 62505136, and 62575139), Fundamental Research Funds for the Central Universities (Grant No. 30923010206), Fundamental Research Funds for the Central Universities (Grant Nos. 2023102001 and 2024202002), National Key Laboratory of Plasma Physics (Grant No. JCKYS2024212804), and Open Research Fund of Jiangsu Key Laboratory of Spectral Imaging and Intelligent Sense (Grant No. JSGPCXZNGZ202401), Project No. WPC3/2022/47/INTENCITY/2024 funded by the National Center for Research and Development (NCBR) under the 3rd Polish-Chinese/Chinese-Polish Joint Research Call (2022).

AUTHOR DECLARATIONS

Conflict of Interest

The authors have no conflicts to disclose.

Author Contributions

Tingxiang Xiong and Yefeng Shu contributed equally to this work.

Tingxiang Xiong: Writing – original draft (equal). **Yefeng Shu**: Writing – original draft (equal). **Ran Ye**: Resources (equal). **Maciej Trusiak**: Supervision (equal). **Malgorzata Kujawinska**: Resources (equal). **Jiasong Sun**: Methodology (equal); Supervision (equal).

Yao Fan: Writing – review & editing (equal). **Chao Zuo**: Supervision (equal).

DATA AVAILABILITY

The data that support the findings of this study are available from the corresponding authors upon reasonable request.

REFERENCES

[1] Y. Park, C. Depeursinge, and G. Popescu, "Quantitative phase imaging in biomedicine," Nat. Photonics **12**, 578–589 (2018).
[2] F. Zernike, "How I discovered phase contrast," Science **121**, 345–349 (1955).
[3] C. J. Mann, L. Yu, C.-M. Lo, and M. K. Kim, "High-resolution quantitative phase-contrast microscopy by digital holography," Opt. Express **13**, 8693–8698 (2005).
[4] Z. Li, J. Sun, Y. Fan, Y. Jin, Q. Shen, M. Trusiak, M. Cywińska, P. Gao, Q. Chen, C. Zuo *et al.*, "Deep learning assisted variational Hilbert quantitative phase imaging," Opto-Electron. Sci. **2**, 220023 (2023).
[5] J. Primot and L. Sogno, "Achromatic three-wave (or more) lateral shearing interferometer," J. Opt. Soc. Am. A **12**, 2679–2685 (1995).
[6] J.-C. Chanteloup, "Multiple-wave lateral shearing interferometry for wave-front sensing," Appl. Opt. **44**, 1559–1571 (2005).
[7] P. Bon, G. Maucort, B. Wattellier, and S. Monneret, "Quadriwave lateral shearing interferometry for quantitative phase microscopy of living cells," Opt. Express **17**, 13080–13094 (2009).
[8] G. Popescu, T. Ikeda, R. R. Dasari, and M. S. Feld, "Diffraction phase microscopy for quantifying cell structure and dynamics," Opt. Lett. **31**, 775–777 (2006).
[9] C. Zuo, Q. Chen, W. Qu, and A. Asundi, "High-speed transport-of-intensity phase microscopy with an electrically tunable lens," Opt. Express **21**, 24060–24075 (2013).
[10] L. Tian and L. Waller, "Quantitative differential phase contrast imaging in an LED array microscope," Opt. Express **23**, 11394–11403 (2015).
[11] N. Shibata, S. D. Findlay, Y. Kohno, H. Sawada, Y. Kondo, and Y. Ikuhara, "Differential phase-contrast microscopy at atomic resolution," Nat. Phys. **8**, 611–615 (2012).
[12] S. B. Mehta and C. J. R. Sheppard, "Quantitative phase-gradient imaging at high resolution with asymmetric illumination-based differential phase contrast," Opt. Lett. **34**, 1924–1926 (2009).
[13] M. Chen, Z. F. Phillips, and L. Waller, "Quantitative differential phase contrast (DPC) microscopy with computational aberration correction," Opt. Express **26**, 32888–32899 (2018).
[14] B. Seong, I. Kim, T. Moon, M. Ranathunga, D. Kim, and C. Joo, "Untrained deep learning-based differential phase-contrast microscopy," Opt. Lett. **48**, 3607–3610 (2023).
[15] M. Kellman, M. Chen, Z. F. Phillips, M. Lustig, and L. Waller, "Motion-resolved quantitative phase imaging," Biomed. Opt. Express **9**, 5456–5466 (2018).
[16] G. Zheng, R. Horstmeyer, and C. Yang, "Wide-field, high-resolution Fourier ptychographic microscopy," Nat. Photonics **7**, 739–745 (2013).
[17] Y. F. Cheng, M. Strachan, Z. Weiss, M. Deb, D. Carone, and V. Ganapati, "Illumination pattern design with deep learning for single-shot Fourier ptychographic microscopy," Opt. Express **27**, 644–656 (2019).
[18] Y. Li, C. Shen, J. Tan, X. Wen, M. Sun, G. Huang, S. Liu, and Z. Liu, "Fast quantitative phase imaging based on Kramers–Kronig relations in space domain," Opt. Express **29**, 41067–41080 (2021).
[19] X. Chen, S. Yao, X. Yan, H. Ding, J. Ma, and C. Yuan, "Single-shot resolution-enhancement quantitative phase imaging based on Kramers–Kronig relations," Opt. Lett. **48**, 3563–3566 (2023).
[20] C. Zuo, J. Li, J. Sun, Y. Fan, J. Zhang, L. Lu, R. Zhang, B. Wang, L. Huang, and Q. Chen, "Transport of intensity equation: A tutorial," Opt. Lasers Eng. **135**, 106187 (2020).
[21] M. Chen, L. Tian, and L. Waller, "3D differential phase contrast microscopy," Biomed. Opt. Express **7**, 3940–3950 (2016).
[22] Y. Fan, J. Sun, Y. Shu, Z. Zhang, Q. Chen, and C. Zuo, "Accurate quantitative phase imaging by differential phase contrast with partially coherent illumination: Beyond weak object approximation," Photonics Res. **11**, 442–455 (2023).
[23] Y. Fan, J. Sun, Q. Chen, X. Pan, M. Trusiak, and C. Zuo, "Single-shot isotropic quantitative phase microscopy based on color-multiplexed differential phase contrast," APL Photonics **4**, 121301 (2019).
[24] Y. Fan, J. Sun, Q. Chen, X. Pan, L. Tian, and C. Zuo, "Optimal illumination scheme for isotropic quantitative differential phase contrast microscopy," Photonics Res. **7**, 890–904 (2019).
[25] H.-H. Chen, Y.-Z. Lin, and Y. Luo, "Isotropic differential phase contrast microscopy for quantitative phase bio-imaging," J. Biophot. **11**, e201700364 (2018).
[26] R. Cao, M. Kellman, D. Ren, R. Eckert, and L. Waller, "Self-calibrated 3D differential phase contrast microscopy with optimized illumination," Biomed. Opt. Express **13**, 1671–1684 (2022).
[27] Y. Fan, C. Zheng, Y. Shu, Q. Fu, L. Xiong, G. Lu, J. Sun, C. Zuo, and Q. Chen, "Aberration-corrected differential phase contrast microscopy with annular illuminations," Opto-Electron. Sci. **4**, 240037 (2025).
[28] J. Jiang, F. Li, F. Yang, W. Yan, and J. Du, "Single-shot color-coded LED microscopy for quantitative differential phase contrast imaging," Opt Laser. Technol. **161**, 109192 (2023).
[29] D. Lee, S. Ryu, U. Kim, D. Jung, and C. Joo, "Color-coded LED microscopy for multi-contrast and quantitative phase-gradient imaging," Biomed. Opt. Express **6**, 4912–4922 (2015).
[30] W. Lee, J.-H. Choi, S. Ryu, D. Jung, J. Song, J.-S. Lee, and C. Joo, "Color-coded LED microscopy for quantitative phase imaging: Implementation and application to sperm motility analysis," Methods **136**, 66–74 (2018).
[31] Z. F. Phillips, M. Chen, and L. Waller, "Single-shot quantitative phase microscopy with color-multiplexed differential phase contrast (cDPC)," PloS One **12**, e0171228 (2017).
[32] S. Liu, C. Zheng, Q. Hao, X. Li, and S. Zhang, "Single-shot quantitative differential phase contrast imaging combined with programmable polarization multiplexing illumination," Opt. Lett. **48**, 3559–3562 (2023).
[33] R. Kalita, W. Flanagan, J. Lightley, S. Kumar, Y. Alexandrov, E. Garcia, M. Hintze, M. Barkoulas, C. Dunsby, and P. M. W. French, "Single-shot phase contrast microscopy using polarisation-resolved differential phase contrast," J. Biophot. **14**, e202100144 (2021).
[34] J. Lim, K. Lee, K. H. Jin, S. Shin, S. Lee, Y. Park, and J. C. Ye, "Comparative study of iterative reconstruction algorithms for missing cone problems in optical diffraction tomography," Opt. Express **23**, 16933–16948 (2015).
[35] Y. Gao and L. Cao, "Motion-resolved, reference-free holographic imaging via spatiotemporally regularized inversion," Optica **11**, 32–41 (2024).
[36] S. Marchesini, H. He, H. N. Chapman, S. P. Hau-Riege, A. Noy, M. R. Howells, U. Weierstall, and J. C. H. Spence, "X-ray image reconstruction from a diffraction pattern alone," Phys. Rev. B **68**, 140101 (2003).
[37] M. Braiki, A. Benzinou, K. Nasreddine, and N. Hymery, "Automatic human dendritic cells segmentation using K-means clustering and Chan-Vese active contour model," Comput. Methods Programs Biomed. **195**, 105520 (2020).
[38] P. Wu, J. Yi, G. Zhao, Z. Huang, B. Qiu, and D. Gao, "Active contour-based cell segmentation during freezing and its application in cryopreservation," IEEE Trans. Biomed. Eng. **62**, 284–295 (2015).
[39] K. Wu, D. Gauthier, and M. D. Levine, "Live cell image segmentation," IEEE Trans. Biomed. Eng. **42**, 1–12 (1995).
[40] K. O. Oyebode and J. R. Tapamo, "Automatic segmentation of cell images by improved graph cut-based approach," J. Biomimetics, Biomater. Biomed. Eng. **29**, 74–80 (2016).
[41] T. Vicar, J. Balvan, J. Jaros, F. Jug, R. Kolar, M. Masarik, and J. Gumulec, "Cell segmentation methods for label-free contrast microscopy: Review and comprehensive comparison," BMC Bioinf. **20**, 360 (2019).
[42] R. Gerhberg and W. Saxton, "A practical algorithm for the determination of phase from image and diffraction plane picture," Optik **35**, 237–246 (1972).
[43] J. R. Fienup, "Reconstruction of an object from the modulus of its Fourier transform," Opt. Lett. **3**, 27–29 (1978).